HHS Public Access

Author manuscript

Neuroimage. Author manuscript; available in PMC 2019 June 06.

Published in final edited form as:

Neuroimage. 2018 October 01; 179: 313–325. doi:10.1016/j.neuroimage.2018.06.013.

Visuocortical changes during a freezing-like state in humans

Maria Lojowska[a,b,*], **Sam Ling**[a,c], **Karin Roelofs**[a,b,1], and **Erno J. Hermans**[a,d,1]

[a]Donders Institute for Brain, Cognition and Behaviour, Nijmegen, The Netherlands [b]Behavioural Science Institute, Radboud University, Nijmegen, The Netherlands [c]Department of Psychological and Brain Sciences, Boston University, Boston, USA [d]Radboud University Medical Center, Nijmegen, The Netherlands

Abstract

An adaptive response to threat requires optimized detection of critical sensory cues. This optimization is thought to be aided by freezing - an evolutionarily preserved defensive state of immobility characterized by parasympathetically mediated fear bradycardia and regulated by the amygdala-periaqueductal grey (PAG) circuit. Behavioral observations in humans and animals have suggested that freezing is also a state of enhanced visual sensitivity, particularly for coarse visual information, but the underlying neural mechanisms remain unclear. We induced a freezing-like state in healthy volunteers using threat of electrical shock and measured threat-related changes in both stimulus-independent (baseline) and stimulus-evoked visuocortical activity to low-vs. high-spatial frequency gratings, using functional MRI. As measuring immobility is not feasible in MRI environments, we used fear bradycardia and amygdala-PAG coupling in inferring a freezing-like state. An independent functional localizer and retinotopic mapping were used to assess the retinotopic specificity of visuocortical modulations. We found a threat-induced increase in baseline (stimulus-independent) visuocortical activity that was retinotopically nonspecific, which was accompanied by increased connectivity with the amygdala. A positive correlation between visuocortical activity and fear bradycardia (while controlling for sympathetic activation), and a concomitant increase in amygdala-PAG connectivity, confirmed the specificity of these findings for the parasympathetically dominated freezing-like state. Visuocortical responses to gratings were retinotopically specific, but did not differ between threat and safe conditions across participants. However, individuals who exhibited better discrimination of low-spatial frequency stimuli showed reduced stimulus-evoked V1 responses under threat. Our findings suggest that a defensive state of freezing involves an integration of preparatory defensive and perceptual changes which may be regulated by a common mechanism involving the amygdala.

[*]Corresponding author. Donders Institute for Brain, Cognition and Behaviour, Nijmegen, The Netherlands. lojowska.maria@gmail.com (M. Lojowska).

[1]Equal contribution to the paper.

Authors' contribution

ML, EJH, KR designed research. ML performed research. ML analyzed data. ML, SL, EJH, KR wrote the paper. All authors approved the final version of the manuscript for submission.

Declaration of interests

None.

Appendix A. Supplementary data

Supplementary data related to this article can be found at https://doi.org/10.1016/j.neuroimage.2018.06.013.

Keywords

Freezing; Functional MRI; Visual perception; Spatial frequency; Fear bradycardia

Introduction

Optimal perception of relevant sensory cues is crucial to avoid harm in threatening situations. This perceptual optimization has been suggested to be aided by *freezing* - an evolutionarily preserved defensive response that prepares the body for a successful countering of threat (Blanchard et al., 2011; Campbell et al., 1997; Fanselow, 1994; Hagenaars et al., 2014; Lojowska et al., 2015; Ohman and Wiens, 2003). Freezing commonly takes place during threat anticipation and is characterized by bodily immobility and a parasympathetically dominated decrease in heart rate, or *fear bradycardia*, in both animals and humans (Fanselow and Lester, 1988; Gladwin et al., 2016; Obrist et al., 1965; Roelofs, 2017; Walker and Carrive, 2003). Behavioral observations suggest that freezing is also a state of enhanced visual sensitivity, specifically for coarse visual information (Blanchard et al., 2011; Lojowska et al., 2015). However, despite the potential relevance of these perceptual changes for threat coping, the underlying neural mechanism remains unclear.

The anticipatory state of freezing is characterized by a specific pattern of sympathetic and parasympathetic autonomic nervous system activity. Whereas concurrent sympathetic activation, as observed for instance in increased pupil size and skin conductance, prepares the body for potential actions (fight-or-flight), parasympathetic dominance serves as a break on the motor system, allowing for threat assessment and decision-making about the most adaptive behavior in given circumstances (Blanchard et al., 2011; Kozlowska et al., 2015). Crucially, because these decisions largely depend on the visual characteristics of a threat (e.g., its ambiguity or magnitude), freezing has been conceptualized as a state of enhanced sensory processing during which an animal gathers relevant visual information (Blanchard et al., 2011; Eilam, 2005; Roelofs, 2017). This has been supported by behavioral observations in rodents that, despite total bodily immobility, show slight head and ear movements suggestive of environmental scanning and increased visual sensitivity (Blanchard et al., 2011). However, whereas much human and animal research has focused on how visual input (e.g., angry faces, conditioned cues) shapes the expression of freezing behavior (Azevedo et al., 2005; Blanchard et al., 2001; Fanselow and Lester, 1988; Gladwin et al., 2016; Hermans et al., 2013; Maren, 2001; Roelofs et al., 2010; Tovote et al., 2015), the neural mechanism underlying the opposite, i.e., how visual processing is altered during the anticipatory state of freezing, remains unclear.

Enhanced visual processing during freezing may be neurally regulated by the amygdala being also involved in the expression of freezing. In particular, fear bradycardia and immobility are regulated through amygdalar efferents to (ventral) periaqueductal grey (PAG) and medulla (Koba et al., 2016; Kozlowska et al., 2015; Tovote et al., 2016; Walker and Carrive, 2003). PAG activation and its functional connectivity with the amygdala have furthermore been linked to fear bradycardia in humans (Hermans et al., 2013). Crucially,

non-human primate work has also demonstrated widespread projections from amygdala to early and ventral visual areas (Amaral et al., 2003; Freese and Amaral, 2005), whereas in humans the amygdala drives enhanced visuocortical responses to emotionally salient stimuli (Anderson, 2001; Vuilleumier et al., 2004). Based on these findings, we hypothesized that the anticipatory state of freezing should be characterized by a preparatory amygdala-driven enhancement in visuocortical activity, even in the absence of visual input.

In addition, experimental work in humans has shown that freezing is associated with enhanced visual perception specifically of coarse visual information, i.e., low-spatial frequencies (Lojowska et al., 2015). This finding is consistent with the observation that the majority of amygdalar projections to the visual cortex are magnocellular and therefore biased toward processing of lower spatial frequency information (Amaral et al., 2003; Freese and Amaral, 2005; Leonova et al., 2003). These anatomical findings are supported by functional evidence where enhanced neural responses to low- relative to high-spatial frequency fearful faces were found in inferior temporal cortex (Vuilleumier et al., 2003), and larger steady-state visual potentials to low-spatial frequency stimuli were observed over occipito-temporal areas following presentation of aversive compared to neutral images (Song and Keil, 2013). We therefore hypothesized that a state of freezing should also be associated with enhanced early visuocortical responses to coarse visual information.

We conducted a functional magnetic resonance imaging (fMRI) study combined with autonomic nervous system measures in which a transient freezing-like state was induced by means of threat of electric shock. An equal number of safe trials was included as control. Threat of electrical shock is a commonly used procedure during which the main concomitants of freezing, i.e., bodily immobility, fear bradycardia and amygdala PAG recruitment have been observed in both animals and humans (Fanselow, 1994; Fanselow and Lester, 1988; Gladwin et al., 2016; Kapp et al., 1979; LeDoux et al., 1988; Liebman et al., 1970; Obrist, 1968; Schneiderman et al., 1966). As measuring physical immobility in an MRI scanner is not feasible, we relied on fear bradycardia and amygdala-PAG coupling (using psychophysiological interaction models) in validating a freezing-like state in the current study.

To test our hypotheses regarding the effect of threat anticipation on stimulus-independent and stimulus-dependent activity in early visual cortices, we recorded early visuocortical activity in the absence of visual stimulation (during threat versus safe *Omission* trials, in which no gratings were presented), as well as in response to peripherally presented gratings (during threat versus safe *Grating* trials, in which maximally three gratings could be presented). Omission trials were used to assess an increase in baseline visuocortical activity without the confounding effect of stimulus presentation, and its modulation by the amygdala. Grating trials were used to examine transient neural responses to relatively low- (3 cycles per degrees, cpd) and high- (6 cpd) spatial frequencies. We carried out an independent localizer and retinotopic mapping to allow for quantification of retinotopically specific (i.e., stimulus location-selective) and nonspecific activity within V1, V2, and V3. We first predicted that if freezing is associated with an amygdala-driven upregulation of baseline activity, we should observe a threat-related increase in visuocortical activity and its functional coupling with the amygdala during Omission trials. Second, if freezing is

associated with enhanced early visuocortical responses to coarse visual information, larger stimulus-evoked activity should be observed to low-spatial frequency gratings on threat versus safe conditions within retinotopically specific voxels in early visual areas.

Materials and methods

Participants

Forty-eight participants participated in this study. Inclusion criteria were: normal or corrected-to-normal vision, no color blindness, no history of psychiatric or neurological treatment, no cardiovascular conditions and no smoking, right-handedness. Fourteen participants were excluded because of not completing the full task (4), inability to tolerate shocks (3, comparable with our previous study with shocks; Lojowska et al., 2015), falling asleep (2, during low demanding tasks of retinotopy and localizer), feeling uncomfortable inside the scanner (2, first-time MRI participants), arrhythmia detected during data acquisition (1), and performance accuracy below 75% during the tilt titration task before the actual experiment (2, comparable with our previous psychophysiological study; Lojowska et al., 2015). The final sample of 34 participants consisted of 19 males and 15 females with the mean age of 23.15 years (range 19–32). Additionally, we removed behavioral outliers, i.e., >3 SD from the mean (maximum of two participants) or tilt offset >20° (which is unlikely to reflect visual sensitivity; maximum of two participants), for all relevant statistical tests. Before participating in the experiment, all participants were required to grant a written informed consent. Participants were reimbursed with 40 euros for their participation in both sessions of the study. This study was approved by the local ethical review board (CMO Region Arnhem-Nijmegen, The Netherlands).

Sample size calculation (G*Power; Faul et al., 2007) revealed that 34 participants were sufficient to detect a medium effect size (for interaction effect threat x SF, $\eta_p^2 = 0.06$) at 80% power. Although only 12 participants were necessary to replicate a relatively large effect size $\eta_p^2 = .17$) found previously for this interaction effect in a similar psychophysiological study (Lojowska et al., 2015), we nevertheless used the same sample size as in this study (34 participants) in order to increase the chance of detecting possibly smaller effects arising from differences between the tasks (e.g., in testing environment).

Stimuli and apparatus

Stimuli—Gabor grating stimuli (Gaussian-enveloped sinusoidal gratings) were generated using MATLAB R2010a, in combination with the Psychophysics Toolbox (Brainard, 1997). Stimuli were displayed on a rear-projection screen using a luminance-calibrated EIKI projector (1024 × 768 resolution, 60 Hz refresh rate) located 75 cm behind the participant's head. Gratings (4.5° × 4.5° size) were presented at 100% Michelson contrast and in two spatial frequencies: 3 and 6 cpd. These frequencies were used because they fall within the sensitive range of magnocellular and parvocellular cells (Leonova et al., 2003), and because the modulatory effect of threat anticipation was previously found for these specific frequencies (Lojowska et al., 2015). The gratings were displayed at 4° eccentricity from the central fixation. A fixation point (size: 0.15°, luminance: 116cd/m^2) was displayed in the

center of a uniform grey background screen (luminance: 76 cd/m^2), and participants were asked to maintain fixation throughout the course of the experiment. During the visual task, this fixation point could change from grey to orange (luminance: 116 cd/m^2) or blue (luminance: 117 cd/m^2), signaling threat or safe conditions. Stimulus parameters were chosen based on the following considerations. Peripheral display was used to avoid ceiling effects and to increase ecological validity of the task, as peripheral detection may be particularly adaptive in threatening situations, where relevant information (e.g., predator approaching from behind) is not immediately accessible to overt attention. 4° eccentricity was used to minimize the bias in spatial frequency processing due to uneven distribution of cones and rods in retina (Purves et al., 2001), and was based on previous psychophysiological work in which discrimination performance for 3 and 6 cpd was comparable at this eccentricity (Rovamo et al., 1978). Furthermore, horizontal presentation was used to avoid a potential difference in spatial frequency processing between upper and lower parts of the visual field (Christman, 1993). Finally, by using the same stimulus parameters (eccentricity, peripheral horizontal presentation, and spatial frequencies) as in previous studies in which threat-induced modulation on spatial frequency processing was found (Bocanegra and Zeelenberg, 2009; Lojowska et al., 2015; Nicol et al., 2013), we hoped to replicate these behavioral effects in the current study. In the visual task, the maximal tilt offset that the gratings could deviate from the vertical orientation was set to 40°. Contrast, size and presentation time of the gratings (100 m s) were chosen to ensure their full visibility while rear-projected in the scanner during the visual task, and to prevent participants from making saccadic eye movements towards the stimuli, which would require about 160 m s (Walker et al., 1997).

Shock administration and physiological measurements

Electric shocks were delivered transcutaneously through the participant's fourth and fifth distal phalanges of the right hand using a 9 V battery-operated MAXTENS 2000 (Bio-Protech, Inc., Wonju, Korea) and standard Ag/AgCl electrodes. The duration of the electrical stimulation was 200 m s, with a 150 Hz repetition of 250 μs pulses. The intensity varied between 0 and 40 V/0–80 mA across 500Ω with 10 steps in total. Shock intensity was adjusted at the individual level to ensure the shocks were unpleasant but not painful. Shock calibration was performed using a standardized staircase procedure comprising 5 shock presentations after each of which the shock intensity was adjusted according to the participant's verbal reports of its unpleasantness on a scale from 1 (not unpleasant) to 5 (very unpleasant). The final shock intensity obtained with this method (mean score: 4.36, SD = .65) was used in the visual orientation discrimination task.

The following physiological measures were recorded: heart rate (HR), pupil size and respiration in both sessions, as well as skin conductance in the second session in which the visual task was carried out. HR was used for offline assessment of the parasympathetically driven decelerative HR responses, whereas pupil size and skin conductance were used as an index of sympathetic activity during the task (Hermans et al., 2013). Heart rate and respiration were additionally used for retrospective image-based correction (RETROICOR) of physiological noise artifacts in BOLD signal in fMRI data (Glover et al., 2000). HR, skin conductance and respiration were acquired using an MR-compatible BrainAmp EXG MR 16

channel recording system (Brain Products, Gilching, Germany). HR was measured using a pulse oximeter that was attached to a fourth distal phalange of the participants' left hand. Skin conductance data were collected with two standard Ag/AgCl electrodes attached to the second and third distal phalanges of the participant's left hand. Respiration data were collected using a respiration belt positioned around the participant's abdomen. Pupil size was measured using a 50 Hz iView system with an MR-compatible eye tracker (MEye Track-LR camera unit, SMI, SensoMotoric Instruments).

MRI data acquisition

MRI data were acquired at the Donders Center for Cognitive Neuroimaging using a 3T Siemens MAGNETOM Skyra MRI scanner (Siemens, Erlangen, Germany). Functional MRI data were acquired using a T2*-weighted gradient-echo EPI sequence and parallel multiband excitation with an acceleration factor of four (TR = 909 m s, TE = 24.6 m s, 60 axial slices acquired in interleaved order, flip angle = 59°, field of view = 212*212 mm, slice thickness = 2 mm with no gap between slices, voxel size = 2 mm isotropic, GRAPPA in-plane acceleration factor of 2). Furthermore, field maps were acquired for each participant to allow for correction of spatial distortions in the BOLD-fMRI images due to magnetic field inhomogeneity (TR = 1020 m s; TE1 = 10 m s; TE2 = 12.46 m s; flip angle = 90°; slice matrix size = 64*64; field of view = 224*224 mm). A high-resolution whole-brain anatomical image was acquired using a T1-weighted Magnetization-Prepared RApid Gradient Echo (MP-RAGE) sequence (TR = 2300 m s; TE = 315 m s; flip angle = 8°; slice matrix size = 256*256; field of view = 256*256*180 mm; voxel size = 0.8 mm isotropic).

Experimental procedure

The entire experiment was divided over two sessions, scheduled 3–4 days apart. The first session consisted of the functional localizer task, retinotopic mapping task, as well as resting state and susceptibility-weighted imaging sequence which were not analyzed for the current study. The second session consisted of questionnaires, a tilt titration task, a shock calibration procedure and the visual task with electric shocks (i.e., the task of primary interest). Participants lay in the scanner in a head-first supine position and viewed the back-projection screen via a mirror mounted on top of the head coil.

The first session started with the functional localizer task. This task comprised flickering gratings presented at 100% contrast in 16 blocks of 38 s each. In each block, a grating (either 3 cpd or 6 cpd) were presented at 4° eccentricity for 9.5 s and with a random phase change between the blocks. The orientation of the gratings was fixed within, but varied between the blocks. We included the following tilt offsets: ±3, ±6, ±10, ±14. Blocks with each orientation were repeated twice. Blocks were separated by a 9.5s grey screen containing only a fixation at the center of the screen. To ensure central fixation during the task, the white fixation in the center of the screen turned black at pseudorandom time points, which prompted a button-press response from participants. The localizer task lasted approximately 14 min.

During the retinotopic mapping task, participants viewed a wedge consisting of a flashing black-and-white checkerboard pattern (3 Hz), first rotating clockwise for 6 cycles and then

anticlockwise for another 6 cycles (at a rotation speed of 36s/cycle). Also during this task, the central fixation changed color from white to black, prompting a button-press response from participants to ensure central fixation.

The second session started with participants completing questionnaires, which were included to enable post-hoc assessment of whether participant samples of our previous behavioral and current fMRI study were comparable (Lojowska et al., 2015). During the tilt titration task, tilt offset was titrated separately for the 3 cpd and 6 cpd stimuli in the same visual orientation task, but without shocks and omission trials. The final staircase thresholds obtained in this task were subsequently used as a starting tilt offset for gratings in the actual experiment (one threshold for 3 cpd stimuli under threat and safe conditions, and one threshold for 6 cpd stimuli under threat and safe conditions). The tilt titration task consisted of 72 gratings in each spatial frequency, taking about 10 min, and was administered in the scanner during the acquisition of the anatomical scan. Subsequently, to adjust shock intensity to individual sensitivity thresholds, participants underwent a shock calibration procedure. This was followed by visual task lasting about 50–60 min, with short breaks in between.

Visual task

Each trial started with a 7 s presentation of the central fixation point, the color of which - blue or orange - indicated either threat or safe conditions (Fig. 1). Color fixation was followed by an ITI of 2–4 s, during which the fixation color changed to grey. A freezing-like state was evoked in the threat condition by a chance of receiving an electric shock, administered to the participant’s fourth and fifth distal phalanges of the right hand. No shocks were administered during the safe condition. Participants received verbal instructions about the association between fixation color and shocks before the start of the experiment. The association between fixation color and threat condition was counterbalanced across participants. 25% of all trials were omission trials, during which only the central fixation was presented. These trials were used to quantify threat-related changes in baseline visuocortical activity. The remaining 75% of all trials were used to probe threat-related changes in neurocortical responses to visual information. To this end, participants performed a visual orientation discrimination task (Lojowska et al., 2015) that required discrimination of the orientation of the gratings under orthogonalized threat and safe conditions. These trials were the same as omission trials with the exception of gratings presented either to the left or right side of the fixation. In total, there were four conditions: threat 3 cpd, threat 6 cpd, safe 3 cpd, and safe 6 cpd. Gratings were presented during the display of an orange or blue fixation for the duration of 100 m s. Up to 3 gratings could be presented in a single trial. The minimum interstimulus interval (ISI) was set to 2 s, allowing for separation of BOLD responses to each grating (Wager and Nichols, 2003). After each grating, participants were required to indicate through button press whether its orientation was left or right relative to vertical. The presentation side, spatial frequency of the gratings and their orientation (left versus right) were counterbalanced between sessions and participants. Participants were instructed to fixate on the central dot during the whole task and avoid excessive blinking when the orange or blue fixation was presented.

To ensure that neurocortical responses to the gratings reflect threat-related manipulations, rather than task difficulty known to increase activity in the visual cortex (Chen et al., 2008), we used an adaptive staircase procedure (QUEST; Watson and Pelli, 1983) allowing to maintain an overall level of 75% accuracy while varying tilt offset in each of the four conditions. This procedure was applied separately for each of the four conditions and the resulting changes in the tilt offsets were used as measures of behavioral performance.

The task was divided into three runs, each consisting of 102 trials (36 safe/threat trials with gratings, 12 safe/threat omission trials and 6 threat trials with shocks). In each run, 36 gratings belonging to each of the four conditions were presented in grating trials. Trials with shock presentation were excluded from the analyses. The trial sequence was fully randomized for each participant to ensure that potential carry-over effects between trial types could not result in a systematic bias. Total duration of the second session was about 2 h. After MRI scanning, participants were asked debriefing questions to assure they understood all instructions (e.g., regarding the association between the fixation color and chance of receiving a shock), and to verify the experimental manipulations (e.g., whether they received shocks and how many, and about the perceived aversiveness of the shocks).

Data analysis

Behavioral and physiological analyses—Behavioral performance was defined as the mean tilt offset required to perform the orientation discrimination task at 75% accuracy, for each of the 4 conditions. The mean was calculated for each run and analyzed using SPSS (IBM SPSS Statistics for Windows, Version 21.0), with run number (1–3), threat condition and spatial frequency as within subject factors. Data of four participants were excluded from the behavioral analysis because of tilt offsets exceeding outlier thresholds (larger than 3 SD when tested separately for 3 cpd and 6 cpd).

The analysis of physiological data was performed offline using in-house software implemented in MATLAB (Matlab, R2013a, The Math-Works, Inc), allowing for visual assessment and removal of signal artifacts. Blinks in pupil data were removed from the signal using linear interpolation. HR data for 6 subjects were discarded due to extensive amount of noise and artifacts (e.g., pulse oximeter fell off the finger during scanning, excessive hand movement, scanner artifacts, poor signal). For similar reasons, skin conductance data of two participants were also removed from the analysis. To assess parasympathetic and sympathetic activity during the visual task, pre-trial baseline-corrected HR responses, pupil size responses, and skin conductance levels (SCL) were calculated for each trial. HR responses were quantified by calculating the mean HR between 2 and 7s following trial onsets corrected for the baseline (mean HR during 25 s prior to stimulus onset). This relatively long baseline window was chosen to account for fluctuations of HR with the respiratory cycle due to respiratory sinus arrhythmia (De Geus et al., 1995). Baseline-corrected pupil size responses were quantified by subtracting the averaged pupil diameter within a 1 s period prior to trial onset (baseline) from the averaged pupil diameter within a period from 2 to 7 s following trial onset. Changes in SCLs were calculated using the same time windows. We reasoned that SCL change is a more appropriate measure of sympathetic arousal in the current block design than conventional scoring of skin

conductance response magnitudes commonly used in event-related designs (Phelps et al., 2001). The difference between HR responses on threat vs. safe conditions (across both grating and omission trials) were analyzed using paired sample *t*-test. As SCLs and pupil responses did not have a normal distribution (Shapiro-Wilk test p-value < .001), the difference between threat and safe conditions for these measures were assessed using a non-parametric permutation *t*-test (with 50,000 permutations).

Because of expected physiological changes during our task (due to threat modulation), we used physiological noise correction in all our fMRI analyses to remove variance in BOLD signal originating from these fluctuations. In this way, any differences between threat and safe trials are more likely to reflect the underlying changes in task-related neural responses rather than physiological fluctuations. We included 10 nuisance regressors for cardiac noise and 10 for respiratory noise, which were specified by calculating fifth-order Fourier models of the cardiac and respiratory phase-related modulation of the BOLD signal (Glover et al., 2000). In addition to these RETROICOR regressors, we calculated regressors for heart rate frequency, heart rate variability, (raw) abdominal circumference, respiratory frequency, respiratory amplitude, and respiration volume per unit time (Birn et al., 2006; van Buuren et al., 2009), yielding a total of 26 nuisance regressors that were subsequently used as regressors of no interests in GLM models.

fMRI data preprocessing

The fMRI data were spatially preprocessed using SPM8 (www.fil.ion.ucl.ac.uk/spm) for analysis in native space. The first five volumes of each session were discarded to allow for T1 equilibration. Field maps were subsequently used to calculate a voxel displacement map (Hutton et al., 2002) for each session which was used for the realignment and dynamic unwarping of functional images. Functional images were realigned to the first image within and across all three runs, yielding head movement parameters (translations and rotations) that were subsequently used as nuisance regressors in the general linear models (GLMs). The mean realigned and unwarped functional image was used to coregister functional images with the T1 image for each participant. Furthermore, inverse normalization parameters were created by segmenting the T1 image into grey matter, white matter and CSF images using a unified probabilistic template registration and tissue classification method (Ashburner and Friston, 2005). These inverse normalization parameters were used to warp MNI-space masks of regions of interest (see below) into native space. All subsequent statistical analyses were performed in native space (i.e., without spatial normalization) and without spatial smoothing.

Functional localizer and regions of interest

To find retinotopically specific voxels in the left and right hemispheres of V1, block regressors for right and left stimulus presentations were constructed and convolved with a canonical hemodynamic response function (HRF). Additional HRF-convolved stick function regressors modeled pseudorandom flickering of the fixation point, the aim of which was to prevented participants from looking at the gratings. Left and right hemisphere responses were found by respective contrasting of beta maps for right vs. left, and left vs. right stimulus presentation. Activations within V1 were defined using the retinotopic boundaries

of V1, delineated based on the retinotopy task and well-established methods (DeYoe et al., 1996; Engel et al., 1997; Sereno et al., 1995) implemented in Freesurfer (http://surfer.nmr.mgh.harvard.edu/). 140 voxels that responded maximally to the contralateral stimulus presentation and belonged to the same cluster (i.e., showing spatial contiguity) were selected in left and right V1, and subsequently used as retinotopically specific ROIs in the analysis of the visual task. 140 voxels corresponded approximately to an activation threshold of $p < 0.05$, uncorrected, using a one-tailed *t*-test. To examine the retinotopic specificity of V1 responses, retinotopically nonspecific ROIs were created by subtracting retinotopically specific ROIs created at a lenient threshold of $p < 0.2$ (uncorrected) from the V1 masks created based on the retinotopy task. Similar procedure was repeated for V2 and V3. Left and right amygdala were defined in native space using automated anatomical segmentation of T1-weighted images in FSL FIRST (http://fsl.fmrib.ox.ac.uk/fsl/fslwiki/FIRST). PAG voxels were delineated on each participant's high-resolution T1 scan using fslview and according to previously described guidelines (Satpute et al., 2013). The resulting PAG ROI had a shape of a hollow cylinder with length of about 10 mm, external diameter of about 6 mm and internal diameter of about 2 mm. The masks were then converted from 4D to 3D space, and resliced to each participant's native space of functional images.

Visual task

For analyses of neurocortical responses in the visual task, separate finite impulse response (FIR) models were created for omission and grating trials. In the model for omission trials, we modeled block responses to threat and safe trials. This model was used to test threat-related changes in baseline visuocortical activity without the confounding effects of visual stimulation. For each run, regressors for threat and omission trials with 14 time bins (TRs) were created starting with the trial onset. Additional 3 regressors of no interest were created for grating threat and safe trials, and threat trials with shocks. For each participant and condition of interest, parameter estimates were extracted from an a priori defined period between 4.5 and 9 s where the peak BOLD response was expected (5–10 TR post-trial onset) for the following visual ROIs: retinotopically specific and nonspecific V1 voxels contralateral and ipsilateral to stimulus presentation. This period allowed for capturing trial-specific BOLD responses without interfering with a subsequent trial which - with minimum ITI of 2 s - could start at 9 s following the onset of the previous trial. Visual inspection of the BOLD signal averaged across threat and safe conditions confirmed that this period captured the BOLD response peak occurring at around 6.5 s following stimulus onset. Changes in baseline V1 activity were tested in a three-way repeated-measures ANOVA with threat condition (threat, safe), retinotopic space (retinotopically specific versus retinotopically nonspecific voxels in V1) and run number (1–3) as within-subject factors. We additionally analyzed the difference in BOLD responses between threat and safe trials for the amygdala and PAG to check whether any threat-induced changes in functional connectivity (see below) are associated with a concurrent overall increase in activation of these regions.

In the second FIR model, we estimated neurocortical responses time-locked to the presentation the gratings. For each run, eight regressors of interest were created representing the following conditions: threat 3 cpd, threat 6 cpd, safe 3 cpd, and safe 6 cpd, for left and right presentations. Gratings to which no responses were given as well as shock trials were

modeled by additional FIR regressors of no interest. For each participant, parameter estimates in a period from 2.7 to 5.4 s following stimulus onset were extracted for each condition. This period allowed for capturing stimulus-evoked BOLD responses peaking around 3–5 s following stimulus onset. This selection was based on visual inspection of the average BOLD responses across all conditions (retinotopically specific and nonspecific voxels, ipsilateral and contralateral to stimulus presentation), and therefore was orthogonal to the results of interests. To validate localizer procedure (i.e., larger BOLD responses were expected in the retinotopically specific compared to nonspecific voxels contralateral to stimulus presentation side) and to assess threat-related changed in V1 responses to 3 cpd gratings, averaged parameter estimates were analyzed with a repeated measured ANOVA with stimulated hemisphere (contralateral versus ipsilateral relative to stimulus presentation), retinotopic space (retinotopically specific versus nonspecific voxels in V1), run number (1–3), threat condition (threat, safe) and SF (3 and 6 cpd) as within-subject factors. In each of these models, we included head motion parameters (3 translations, 3 rotations) from realignment, 26 physiological noise regressors, high-pass filtering (1/128 Hz cut-off) to remove low-frequency signal drifts, and AR(1) serial correlation correction.

Effective connectivity analysis

To test whether threat of shock leads to the predicted changes in connectivity between the amygdala with V1 and PAG, we performed a psychophysical interaction (PPI) analysis (Gitelman et al., 2003). We used voxels in the left and right amygdala as seperate seed regions, which were defined by individually created masks in native space (see above). We calculated the first eigenvariates of the time series within left and right amygdala for each participant and run. After deconvolution, these were multiplied by a psychological component (threat vs. safe omission trial regressor) to obtain a run-specific PPI term, which was subsequently re-convolved with the HRF. A GLM with three regressors for each session (PPI term, seed-region eigenvariate, and psychological component) was conducted to calculate participant-specific parameter estimate maps for the PPI term. These parameter estimates were averaged across retinotopically specific and retinotopically nonspecific voxels within V1, as well as within PAG. The resulting values, which represent participant-specific estimates of threat-related changes in connectivity, were tested for statistical significance across participants using a repeated measures ANOVA for each ROI.

Results

Peripheral physiological responses

We first analyzed peripheral physiological responses to verify the effectiveness of our threat manipulation. First, we found a significantly lower heart rate on threat versus safe conditions, $t(1,27) = 5.56$, $p < 001$, $\eta_p^2 = .54$, verifying that our threat-of-shock manipulation evoked fear bradycardia. Furthermore, we also found a significant increase in pupil dilation, $t(1,33) = 5.09$, $p < .001$, $\eta_p^2 = .44$, as wellasSCL, $t(1,31) = 3.81$, $p = .001$, $\eta_p^2 = .32$, indicating the concurrent presence of sympathetic activation during threat conditions. However, given the long duration of the task (approximately an hour), there was a risk of habituation effects with parasympathetic and sympathetic responses decreasing over time.

Indeed, a repeated-measures ANOVA with run number as a within-subject factor showed a main effect of run number on differential scores (threat - safe) of HR responses, $F(2,54) = 9.12$, $p < .001$, $\eta_p^2 = .25$, pupil dilation responses, $F(2,66) = 27.08$, $p < .001$, $\eta_p^2 = .45$, and SCLs, $F(2,62) = 24.67$, $p < .001$, $\eta_p^2 = .44$ (Fig. 2). A further planned linear contrast revealed a significant linear trend for all physiological responses, namely HR responses $F(1,27) = 10.04$, $p = .004$, $\eta_p^2 = .27$, pupil dilation responses, $F(1,33) = 61.90$, $p < .001$, $\eta_p^2 = .65$, and SCRs, $F(1,31) = 41.31$, $p < .001$, $\eta_p^2 = .57$, confirming that the magnitude of both sympathetic and parasympathetic responses to threat relative to safe conditions decreased over time. Habituation of physiological responses to threat of shock is accompanied by a reduction of subjectively perceived shock aversiveness toward the end of the task (average rating of shock aversiveness = 2.88 on a scale from 1 to 5) compared to during shock calibration (M = 4.38). Because these manipulation checks indicate that threat of shock was successful and had the strongest effect in the first run, we included run number as a factor in all further analyses.

Behavioral results

To test if discrimination of the gratings differed as a function of threat condition, we conducted a 2 (threat condition: threat, safe) × 2 (spatial frequency: 3 cpd, 6 cpd) × 3 (run number, 1–3) repeated-measures ANOVA with tilt offset as dependent variable. First, we found a main effect of spatial frequency, $F(1,29) = 12.18$, $p = .002$, $\eta_p^2 = .30$, with 3 cpd gratings (mean tilt offset = 2.12) discriminated better than the 6 cpd gratings (mean tilt offset = 3.28) which conforms with generally higher sensitivity to lower spatial frequencies when presented in the periphery (Díez-Ajenjo and Capilla, 2010; Rovamo et al., 1978). There was no main effect of threat, $F(1,29) = 2.06$, $p = .16$, nor an interaction between threat condition and spatial frequency, $F(1,29) = 3.08$, $p = .09$. However, there was a significant interaction between threat condition, spatial frequency, and run number, $F(2,58) = 4.02$, $p = .023$, $\eta_p^2 = .12$, indicating time-dependent differences in the effects of threat on tilt offset of the gratings.

Given that we used an adaptive staircase procedure (QUEST) that started at the same tilt offset for both threat conditions within each spatial frequency, threat-related changes could become evident as a difference in tilt offset between the two threat conditions building up over time within each spatial frequency (Table 1). We tested this by examining the linear trend across runs within the interaction between threat condition and run number for each spatial frequency. Indeed, a steeper linear trend for threat versus safe conditions was found for 3 cpd stimulus, $F(1,29) = 6.14$, $p = .019$, $\eta_p^2 = .17$, but not for the 6 cpd stimulus, $F(1,29) = 2.00$, $p = .17$, $\eta_p^2 = .065$, indicating that, the decrease in tilt offset (i.e., increase in performance) for the 3 cpd stimulus was steeper in the threat condition than in the safe condition.

Neuroimaging results

Threat effects on baseline V1 activity—To test our first (stimulus-independent) hypothesis that freezing is a state associated with an increase in baseline V1 activity, we compared the amplitude of BOLD responses in V1 on threat vs. safe trials during omission trials where no gratings were presented. To assess retinotopic specificity of these changes, we further compared the response of retinotopically specific (i.e., stimulus-responsive) and nonspecific voxels within V1. A three-way repeated-measures ANOVA with threat condition (threat, safe), retinotopic space (retinotopically specific versus retinotopically nonspecific voxels in V1) and run number (1–3) as within-subject factors revealed no significant main effect of threat condition, $F(1,33) = 1.25$, $p = .27$, $\eta_p^2 = .19$. However, the effect of threat on the activation of V1 differed between runs, as indicated by a significant interaction between threat condition and run number, $F(2,66) = 3.28$, $p = .044$, $\eta_p^2 = .60$ (Fig. 3 A). There was a significantly higher baseline V1 activity in threat versus safe conditions in run 1, $F(1,33) = 6.50$, $p = .016$, $\eta_p^2 = .16$, but not in run 2 and run 3 (ps > .05), conforming to the pattern of physiological habituation. A follow-up analysis for run 1 revealed that significantly higher baseline activity was observed in both retinotopically specific, $t(33) = 2.34$, $p = .026$, $\eta_p^2 = .14$, and nonspecific voxels, $t(33) = 2.73$, $p = .010$, $\eta_p^2 = .18$, and that the difference in threat effects between the two retinotopic areas was nonsignificant [interaction between threat condition and retinotopic areas: $F(1,33) = 2.08$, $p = .15$, $\eta_p^2 = .06$]. Thus, the observed threat-related increase in baseline V1 activity appears to be retinotopically nonspecific. A summary of the brain regions from a whole-brain analysis for run 1 (where threat-related effects were found in the above native-space FIR-model analysis) are reported in the Supplementary Material.

Next, to test if the threat-induced increase in baseline V1 activity is associated with functional coupling with the amygdala, we performed a PPI analysis between these two regions. Threat-related changes in connectivity strength were assessed by averaging parameter estimates for a PPI term expressing the threat-related change in connectivity with the amygdala for two regions of interest: retinotopically specific V1 voxels and retinotopically nonspecific V1 voxels. The resulting participant-specific averages were tested using a repeated-measures ANOVA with retinotopic space (retinotopically specific versus nonspecific V1 voxels), run number (1–3), seed region (left versus right amygdala), and hemisphere (left, right V1) as within-subject factors. As predicted, we found that threat of shock led to an increase in connectivity between the amygdala and V1, $F(1,33) = 19.33$, $p < .001$, $\eta_p^2 = .37$ (Fig. 4). This threat-induced increase in connectivity did not differ between retinotopically specific and nonspecific voxels, $F(1,33) = 3.02$, $p = .092$, $\eta_p^2 = .084$, or between runs, $F(2,66) = .83$, $p = .44$, $\eta_p^2 = .025$. A follow-up analysis confirmed that the threat-related increase in connectivity was indeed observed for both retinotopically specific [one sample *t*-test: $t(33) = 4.40$, $p < .001$, $\eta_p^2 = .37$], and nonspecific voxels [one-sample *t*-test: $t(33) = 4.16$, $p < .001$, $\eta_p^2 = .34$]. We also found no interaction between these two

factors, $F(2,66) = 1.92$, $p = .15$, $\eta_p^2 = .055$. These findings indicate that the observed connectivity increases were neither retinotopically specific nor time dependent. Taken together, threat of shock resulted in a retinotopically nonspecific increase of baseline activity in early visuocortical areas which was associated with an increase in functional coupling with the amygdala.

ReLationship between visuocorticaL changes and defensive responses to threat

To test the hypothesis that physiological and perceptual changes are part of an integrated defensive response, we first tested whether the magnitude of change in BOLD responses between threat and safe trials correlated with threat-induced changes in heart rate (combined across both Grating and Omission trials). We found a significant negative correlation between threat-induced heart rate change and change in baseline activity in V1, $r(26) = -.41$, $p = .030$ (Fig. 3B). Crucially, this correlation remained significant when controlling for variance associated with sympathetic responses, i.e., threat-induced changes in SCLs and pupil dilation, $r(22) = -.42$, $p = .033$ (tested across all runs). Furthermore, there was no significant correlation between threat-related responses in V1 and either SCL, $\rho(30) = -.15$, $p = .40$, or pupil dilation responses, $\rho(32) = -.19$, $p = .26$. Thus, participants with stronger fear bradycardia also demonstrated larger threat-related increase in V1 activity, and these association remained significant when controlling for concurrent sympathetic activation.

Second, we tested whether the observed increase in functional connectivity between the amygdala and visuocortical areas was accompanied by an increase in functional connectivity between the amygdala and PAG. Threat-related changes in connectivity strength between the amygdala and PAG were assessed by averaging the parameter estimates for a PPI term for the PAG. In line with previous reports (Hermans et al., 2013), a repeated-measures ANOVA with threat condition, run number and seed region (left, right amygdala) as within subject factors revealed a threat-related increase in connectivity between the amygdala and PAG, $F(1,33) = 7.66$, $p = .009$, $\eta_p^2 = .18$, which did not differ between runs, $F(1,33) = .93$, $p = .40$, $\eta_p^2 = .027$ (Fig. 4). Together, the correlation between threat-related changes in baseline V1 activity and fear bradycardia, and the increase in functional connectivity of the amygdala with both V1 and PAG supports the notion of integrated visual and defensive responses.

Additional control analysis for the amygdala activation revealed a significant interaction between threat condition and run number, $F(2,66) = 4.87$, $p = .011$, $\eta_p^2 = .13$, with a significant difference between threat and safe trials present only in the first run [run1: $t(33) = 3.43$, $p = .002$; run2: $t(33) = -.26$, $p = .79$; run 3: $t(33) = -.35$, $p = .73$]. No main effect of threat condition, $F(1,33) = .072$, $p = .79$, $\eta_p^2 = .002$, or an interaction between threat and run number, $F(2,66) = .20$, $p = .82$, $\eta_p^2 = .006$, was observed for PAG activation.

Transient V1 responses to low- and high-spatial frequency gratings under threat

In order to address our second hypothesis concerning stimulus-dependent visuocortical activity, we tested whether low-spatial frequency gratings were associated with increased stimulus-evoked activity within retinotopically specific voxels under threat in V1. To this

end, we first validated our localizer procedure. A repeated-measures ANOVA with stimulated hemisphere (contralateral versus ipsilateral relative to stimulus presentation), retinotopic space (retinotopically specific versus nonspecific voxels in V1), run number (1−3), threat condition (threat, safe) and spatial frequency (3 and 6 cpd) as within-subject factors revealed a significant interaction between stimulated hemisphere and retinotopic space, $F(1,29) = 37.18$, $p < .001$, $\eta_p^2 = .56$. This interaction was driven by significantly larger BOLD responses in retinotopically specific versus retinotopically nonspecific voxels contralateral to stimulus presentation, $F(1,29) = 24.12$, $p < .001$, $\eta_p^2 = .45$, but not on the ipsilateral side, $F(1,29) = 3.46$, $p = .073$, $\eta_p^2 = .11$ (Fig. 5). These results confirm that the localizer procedure was successful.

Next, we examined the amplitude of BOLD responses to low- and high-spatial frequency gratings in retinotopically specific V1 voxels. A repeated-measures ANOVA with threat condition, spatial frequency and run number revealed a significant main effect of spatial frequency, $F(1,29) = 4.93$, $p = .034$, $\eta_p^2 = .014$, with 3 cpd gratings evoking higher responses than 6 cpd gratings. However, for both spatial frequencies, the difference in amplitude of BOLD responses between threat and safe trials was not significantly different, $F(1,29) = .46$, $p = .50$, $\eta_p^2 = .016$, and did not change as a function of run number $F(2,58) = 2.29$, $p = .11$, $\eta_p^2 = .073$.

In spite of the lack differences between threat and safe conditions, we were still interested in whether the magnitude of threat-induced change in event-related responses would be related to visual discrimination performance. We therefore tested the correlation between threat-related changes in performance (threat - safe conditions) with the underlying stimulus-evoked responses in retinotopically specific V1 voxels, for both low- (3 cpd) and high-(6 cpd) spatial frequency gratings. We found that threat-related improvements in performance on the 3 cpd stimulus (larger difference in tilt offset between threat and safe condition) was associated with smaller stimulus-evoked activity in retinotopically specific voxels, $r(30) = .49$, $p = .008$ (Fig. 6). No significant correlation was found for the 6 cpd stimulus, $\rho(29) = .064$, $p = .73$. These two correlations differed at trend level ($z = 1.69$, $p = .091$), implying that the effect of threat on the relationship between behavioral performance and visual activity was marginally stronger for LSF than HSF gratings. Together, these results show that although V1 responses to low-spatial frequency gratings were on average comparable on threat and safe trials, threat-induced reductions in neural responses were associated with improved discrimination of low-spatial frequency gratings.

Threat modulation of stimuLus-independent and stimulus-evoked responses in V2 and V3

To examine whether the observed effects of threat of shock are specific to V1, we extended our analyses to include retinotopically defined areas V2 and V3. Similar threat-induced effects were observed across V1, V2 and V3, i.e., a retinotopically nonspecific increase in baseline activity in run 1, $F(1,33) = 5.81$, $p = .022$, $\eta_p^2 = .15$, and increased functional connectivity with the amygdala, $F(1,33) = 19.20$, $p < .001$, $\eta_p^2 = .37$, neither of which

differed between visual areas (all $F < 1$). We also found positive relationships between stronger fear bradycardia and threat-induced increases in baseline activity, similar to V1, in both V2 [$t(24) = -.49$, $p = .010$] and V3 [$t(24) = -.45$, $p = .022$], both controlling for SCL changes and pupil dilation. Furthermore, no threat-related modulation of event-related responses to the gratings, and their relation with behavioral performance ($p > .05$), were observed in V2 and V3, $F(2,66) = 1.41$, $p = .25$, $\eta_p^2 = .041$. As in V1, we did find clear evidence of retinotopic specificity of event-related responses across all three visual areas, as evidenced by a retinotopic space by hemisphere interaction, $F(1,33) = 50,5$, $p < .001$, $\eta_p^2 = .60$, which did not differ between regions ($F < 1$). In sum, findings for V2 and V3 were largely identical to V1.

Discussion

The goal of the present study was to identify the neural mechanisms underlying behavioral observations of enhanced visual sensitivity during an anticipatory state of freezing. The presence of threat-induced fear bradycardia, a parasympathetically dominated response characteristic of freezing (Fredericks et al., 1974; Koba et al., 2016; Kozlowska et al., 2015; Obrist, 1968), as well as an increase in functional connectivity between amygdala and PAG, core regions involved in expression of freezing in animals (Fanselow, 1994; Fanselow and Lester, 1988; Kapp et al., 1979; LeDoux et al., 1988; Liebman et al., 1970; Schneiderman et al., 1966), implies a successful induction of a freezing-like defensive state, although directly measuring immobility was not possible given the constraints of an MRI environment. First, we found that threat of shock resulted in a retinotopically nonspecific increase in baseline visuocortical activity accompanied by a concurrent increase in functional connectivity with the amygdala. The magnitude of the threat-related increase in baseline visuocortical activity correlated with fear bradycardia. Second, better discrimination of low-spatial frequency (3 cpd) gratings under threat was associated with reduced responses in V1 voxels retinotopically specific to the location of the gratings.

Threat of shock resulted in an increase of baseline visuocortical activity. This finding is in line with previous studies using a threat anticipation procedure in which increased early visual responses were observed during phasic (Keil et al., 2007; Song and Keil, 2013; Stolarova et al., 2006; Thigpen et al., 2017) as well as prolonged (Herrmann et al., 2016; Sege et al., 2017; Straube et al., 2007) presentation of conditioned cues predictive of aversive outcomes. However, although threat anticipation commonly evokes freezing (Fanselow and Lester, 1988), the lack of concurrently acquired state-specific autonomic and neural measures in those studies makes it difficult to generalize these findings to freezing. In addition, because the anticipatory stimuli (e.g., signs) were constantly displayed during anticipatory threat periods, the contribution of anticipatory versus stimulus-driven processing to enhanced visuocortical responses remains unclear in those studies. Our study extends these findings by linking an anticipatory increase in baseline visuocortical activity to defensive responses characteristic of freezing, and by showing that this process is independent of bottom-up visual stimulation.

The upregulation of baseline visuocortical activity under threat was associated with concurrent recruitment of defensive reactions characteristic of a state of freezing. Two findings support this notion. First, enhanced activation of early visual areas (V1, V2, and V3) under threat was associated with stronger fear bradycardia, a parasympathetically dominated response observed during freezing (Fredericks et al., 1974; Koba et al., 2016; Kozlowska et al., 2015; Lang et al., 1997; Obrist et al., 1965). In agreement with earlier work showing neural correlates of fear bradycardia (Hermans et al., 2013) and a correlation between low-spatial frequency perception and fear bradycardia (Lojowska et al., 2015), this association was statistically independent of simultaneously observed sympathetic activation indexed by larger skin conductance and pupil dilation responses under threat. Second, a threat-related increase in functional connectivity between the amygdala and PAG - main regions involved in expression of freezing in animals (Fanselow, 1994; Fanselow and Lester, 1988; Kapp et al., 1979; LeDoux et al., 1988; Liebman et al., 1970; Schneiderman et al., 1966), was associated with concomitant increase in functional coupling between the amygdala and early visual areas. A limitation of the current study is that, due to inherent limitations of an MRI environment, it was not possible to measure physical immobility. Such a measure would have allowed for additional validation of the current results for the state of freezing. However, the close association of fear bradycardia and amygdala-PAG coupling with physical immobility in previous work in the context of threat anticipation, in both animals and humans (Applegate et al., 1983; Fanselow, 1994; Gladwin et al., 2016; Gozzi et al., 2010; Kozlowska et al., 2015; Niermann et al., 2018; Roelofs, 2017; Roelofs et al., 2010; Tovote et al., 2016) indicates the presence of a similar defensive state. Future neuroimaging studies on visuocortical changes during freezing may make use of EEG, which may be feasible to combine with direct measurements of mobility using a stabilometric platform (Gladwin et al., 2016).

The amygdala may be a core region involved in the coordination of visual and defensive processes during freezing. Based on anatomical evidence in non-human primates, the observed increase in stimulus-independent visual cortex activity may be driven by modulatory projections from the basal nucleus of the amygdala to early visual areas (Amaral et al., 2003; Freese and Amaral, 2005, 2006). The existence of amygdala-visual connections in humans has been evidenced by morphological changes in the visual areas (Boes et al., 2012), and the absence of otherwise increased responses in the visual cortex to fearful and arousing stimuli in patients with amygdala damage (Anderson, 2001; Vuilleumier et al., 2004). Simultaneous projections of the central nucleus of the amygdala to PAG, on the other hand, are crucial for the expression of fear bradycardia and bodily immobility during animal freezing (Applegate et al., 1983; Gozzi et al., 2010; Kapp et al., 1979; Kim et al., 1993; LeDoux et al., 1988; Liebman et al., 1970; Tovote et al., 2016; Vianna et al., 2001; Walker and Carrive, 2003). In particular, lesions to the amygdala or ventral PAG reduced bodily immobility and fear bradycardia during threat anticipation (e.g., fear conditioning) in animals (Carrive, 1993; Kapp et al., 1979; Kim et al., 1993; LeDoux et al., 1988; Liebman et al., 1970; Vianna et al., 2001), and the activation of the PAG was associated with stronger fear bradycardia in humans (Hermans et al., 2013). In line with these findings, our results support the view that the anticipatory visual processes under threat may be integrated with

defensive responses specific for the state of freezing through a common neural mechanism involving the amygdala.

What could be the functional relevance of a spatially nonspecific increase in baseline visuocortical activity during freezing? One possibility is that this increase reflects a preparatory state that may facilitate visual processing of relevant stimuli across the entire visual field. This notion is consistent with the observation that freezing commonly takes place during anticipation of potential threats or in ambiguous environments (Eilam, 2005) where the uncertainty of threat may require higher sensitivity to all spatial locations. In our study, this facilitation may be evidenced by the striking association between *reduced* neural responses to low-spatial frequency gratings in retinotopically specific regions and *enhanced* discrimination performance for these stimuli. This correlation cannot be taken to indicate that attention was directed away from the peripheral gratings by the central threat cue (fixation color), because participants with a smaller threat-induced increase in BOLD-responses would then be expected to perform worse, not better. While entirely speculative at this point, a possible explanation for this finding could be that the reduced activity may reflect a smaller prediction error occurring when a bottom-up visual input matches stimulus expectations, which are thought to sharpen stimulus representations and suppress neural responses inconsistent with them (Keller et al., 2012; Kok et al., 2012; Lee and Mumford, 2003). Accordingly, a threat-related increase in baseline activity found here may reflect a magnocellular input from the amygdala, which would enhance visual representations of coarse features, resulting in reduced visual responses upon their presentation. The modulatory effect of amygdala projections on neural responses is supported by their physiological properties, i.e., their termination in superficial and deep layers of the visual cortex, which is also characteristic for feedback projections from higher to lower visual areas (Freese and Amaral, 2005, 2006). Such a mechanism would also explain an otherwise contradictory observation of increased early visuocortical responses to lower spatial frequency stimuli following a brief presentation of an arousing image where no threat anticipation was induced (Song and Keil, 2013). The prediction error explanation, however, cannot be directly supported by the current findings. Future studies utilizing, for instance, multi-voxel pattern analyses or electrophysiological recordings may be able to establish whether the observed threat-related increase in baseline visuocortical activity indeed reflects preparatory activity in lower-spatial frequency sensitive voxels (Henriksson et al., 2008; Issa et al., 2000).

One may argue that increased visuocortical activation observed independently of stimulus presentation reflects noradrenergic modulation by arousal. Indeed, increased noradrenergic activity was previously observed during shock anticipation and indexed by pupil dilation (Joshi et al., 2016; Tsuda et al., 1989). Animal studies have shown that these state-dependent elevations of norepinephrine increase the signal-to-noise ratio of visuocortical neurons (Polack et al., 2013; Vinck et al., 2015), and their sensitivity to preferred visual input (Polack et al., 2013). However, although pupil dilation was also observed in the current study, it was not related to threat-related changes in visuocortical activity. Instead, our data show that a threat-related increase in baseline activity was associated with parasympathetically controlled fear bradycardia. As we found in previous work showing an association between parasympathetic activity and PAG activation (Hermans et al., 2013), this

correlation remained significant when partialing out variance associated with pupil dilation. Thus, our stimulus-independent effects within visual cortices suggest that threat anticipation evokes a pattern of modulation that is qualitatively different from pure noradrenergic activity, perhaps involving cholinergic activity that is strongly associated with the parasympathetic nervous system and is also known to modulate early visual cortices (Soma et al., 2013).

We cannot exclude the possibility that the initial part of the observed threat-induced fear bradycardia involves an orienting response being also characterized by a decelerative heart rate response (Kapp et al., 1979). However, while the orienting response is typically induced by a sudden change in the environment (e.g., cue onset), freezing commonly occurs during threat anticipation after the cue has been evaluated as threatening, and is often associated with a relatively stronger and more prolonged heart rate deceleration than the orienting response (Bradley et al., 2001; Gabrielsen et al., 1985; Hagenaars et al., 2014; Lang et al., 1997; Pavlov, 1927). Because our findings concern the entire anticipatory phase following onset of the threat cue, they are unlikely to reflect only orienting.

In contrast to previous observations (Bocanegra and Zeelenberg, 2009; Song and Keil, 2013), neither an impairment in higher spatial frequency perception nor differences in neural responses to these stimuli under threat were observed in the current study. Although a threat-related impairment of perception for higher spatial frequency stimuli has been proposed to rely on a neural mechanism involving a cross-inhibition between magnocellular and parvocellular cells in the visual system (Bocanegra and Zeelenberg, 2009), no direct psychophysiological evidence currently exists to support this claim. Alternatively, the fact that current and other findings show specific improvement in lower spatial frequencies in the absence of a higher spatial frequency impairment (Lee et al., 2014; Vuilleumier et al., 2003) may suggest that these two processes are rather independent and may therefore not always co-occur. Future studies should establish what additional factors, especially those impairing perception of higher-spatial frequencies, such as pupil dilation (Campbell and Green, 1965), may contribute to threat-related shifts in spatial frequency perception.

To conclude, our data demonstrate that an anticipatory freezing-like defensive state in humans is associated with visuocortical changes that may contribute to changes in visual sensitivity during this defensive state. These visuocortical changes coincide with simultaneously recruited defensive responses which may be regulated through a common neural mechanism involving the amygdala. These results also emphasize the importance of anticipatory threat states in visual perception, and open the way for further research on their role in modulating visual sensitivity to specific visual input such as coarse visual information.

Supplementary Material

Refer to Web version on PubMed Central for supplementary material.

Acknowledgements

The authors would like to thank Ramona Barte and Paul Gaalman for their valuable help with data acquisition.

Funding

KR was supported by a starting grant from the European Research Council (ERC_StG 2012_313749), also funding ML, and by VICI grant (#453-12-001) from the Netherlands Organization for Scientific Research (NWO). EJH was supported by a consolidator grant from the European Research Council (ERC-2015-CoG 682591). SL was supported by National Institutes of Health Grant EY028163.

References

Amaral DG, Behniea H, Kelly JL, 2003 Topographic organization of projections from the amygdala to the visual cortex in the macaque monkey. Neuroscience 118 (4), 1099–1120. 10.1016/s0306-4522(02)01001-1. [PubMed: 12732254]

Anderson AKP,E.A., 2001 Lesions of the human amygdala impair enhanced perception of emotionally salient events. Nature 411, 305–309. [PubMed: 11357132]

Applegate CD, Kapp BS, Underwood MD, McNall CL, 1983 Autonomic and somatomotor effects of amygdala central N. stimulation in awake rabbits. Physiol. Behav 31 (3), 353–360. [PubMed: 6635005]

Ashburner J, Friston KJ, 2005 Unified segmentation. Neuroimage 26 (3), 839–851. [PubMed: 15955494]

Azevedo TM, Volchan E, Imbiriba LA, Rodrigues EC, Oliveira JM, Oliveira LF, et al., 2005 A freezing-like posture to pictures of mutilation. Psychophysiology 42 (3), 255–260. 10.1111/j.1469-8986.2005.00287.x. [PubMed: 15943678]

Birn RM, Diamond JB, Smith MA, Bandettini PA, 2006 Separating respiratory-variation-related fluctuations from neuronal-activity-related fluctuations in fMRI. Neuroimage 31 (4), 1536–1548. 10.1016/j.neuroimage.2006.02.048. [PubMed: 16632379]

Blanchard, Griebel G, Pobbe R, Blanchard RJ, 2011 Risk assessment as an evolved threat detection and analysis process. Neurosci. Biobehav. Rev 35 (4), 991–998. 10.1016/j.neubiorev.2010.10.016. [PubMed: 21056591]

Blanchard DC, Griebel G, Blanchard RJ, 2001 Mouse defensive behaviors: pharmacological and behavioral assays for anxiety and panic. Neurosci. Biobehav. Rev 25, 205–218. [PubMed: 11378177]

Bocanegra, Zeelenberg R, 2009 Emotion improves and impairs early vision. Psychol. Sci 20 (6), 707–713. 10.1111/j.1467-9280.2009.02354.x. [PubMed: 19422624]

Boes AD, Mehta S, Rudrauf D, Van Der Plas E, Grabowski T, Adolphs R, Nopoulos P, 2012 Changes in cortical morphology resulting from long-term amygdala damage. Soc. Cognit. Affect Neurosci 7 (5), 588–595. 10.1093/scan/nsr047. [PubMed: 21896493]

Bradley MM, Codispoti M, Cuthbert BN, Lang PJ, 2001 Emotion and motivation I: defensive and appetitive reactions in picture processing. Emotion 1 (3), 276–298. 10.1037/1528-3542.1.3.276. [PubMed: 12934687]

Brainard DH, 1997 The Psychophysics Toolbox. Spatial Vis. 10 (4), 433–436. 10.1163/156856897X00357.

Campbell BA, Wood G, McBride T, 1997 Origins of orienting and defensive responses: an evolutionary perspective. In: Lang PJ, Simons RF, Balaban MT (Eds.), Attention and Orienting: Sensory and Motivational Processes, pp. 41–67.

Campbell FW, Green DG, 1965 Optical and retinal factors affecting visual resolution. J. Physiol. (London) 181 (3), 576–593. [PubMed: 5880378]

Carrive P, 1993 The periaqueductal gray and defensive behavior: functional representation and neuronal organization. Behav. Brain Res 58 (1–2), 27–47. [PubMed: 8136048]

Chen Y, Martinez-Conde S, Macknik SL, Bereshpolova Y, Swadlow HA, Alonso JM, 2008 Task difficulty modulates the activity of specific neuronal populations in primary visual cortex. Nat. Neurosci 11 (8), 974–982. 10.1038/nn.2147. [PubMed: 18604204]

Christman SD, 1993 Local-global processing in the upper versus lower visual fields. Bull. Psychonomic Soc 31 (4), 275–278.

De Geus EJC, Willemsen GH, Klaver CH, Van Doornen LJ, 1995 Ambulatory measurement of respiratory sinus arrhythmia and respiration rate. Biol. Psychol 41, 205–227. [PubMed: 8608201]

DeYoe AE, Carman GJ, Bandettini P, Glickman S, Wieser J, Cox R, et al., 1996 Mapping striate and extrastriate visual areas in human cerebral cortex. Proc. Natl. Acad. Sci. U. S. A 93 (6), 2382–2386. [PubMed: 8637882]

Díez-Ajenjo MA, Capilla P, 2010 Spatio-temporal contrast sensitivity in the cardinal directions of the colour space. A review. Journal of Optometry 3 (1), 2–19. 10.3921/joptom.2010.2.

Eilam D, 2005 Die hard: a blend of freezing and fleeing as a dynamic defense-implications for the control of defensive behavior. Neurosci. Biobehav. Rev 29 (8), 1181–1191. 10.1016/j.neubiorev.2005.03.027. [PubMed: 16085311]

Engel SA, Glover GH, Wandell BA, 1997 Retinotopic organization in human visual cortex and the spatial precision of functional MRI. Cerebr. Cortex 7 (2), 181–192.

Fanselow MS, 1994 Neural organization of the defensive behavior system responsible for fear. Psychonomic Bull. Rev 1 (4), 429–438. 10.3758/BF03210947.

Fanselow MS, Lester LS, 1988 A functional behavioristic approach to aversively motivated behavior: predatory imminence as a determinant of the topography of defensive behavior In: Bolles RC, Beecher MD (Eds.), Evolution and Learning. Lawrence Erlbaum Associates, Hillsdale: NJ, pp. 185–212.

Faul F, Erdfelder E, Lang AG, Buchner A, 2007 G*Power 3: a flexible statistical power analysis program for the social, behavioral, and biomedical sciences. Behav. Res. Meth 39, 175–191.

Fredericks A, Moore JW, Metcalf FU, Schwaber JS, Schneiderman N, 1974 Selective autonomic blockade of conditioned and unconditioned heart rate changes in rabbits. Pharmacol. Biochem. Behav 2 (4), 493–501. [PubMed: 4607771]

Freese JL, Amaral DG, 2005 The organization of projections from the amygdala to visual cortical areas TE and V1 in the macaque monkey. J. Comp. Neurol 486 (4), 295–317. 10.1002/cne.20520. [PubMed: 15846786]

Freese JL, Amaral DG, 2006 Synaptic organization of projections from the amygdala to visual cortical areas TE and V1 in the macaque monkey. J. Comp. Neurol 496 (5), 655–667. 10.1002/cne.20945. [PubMed: 16615120]

Gabrielsen GW, Blix AS, Ursin H, 1985 Orienting and freezing responses in incubating ptarmigan hens. Physiol. Behav 34, 925–934. [PubMed: 4059382]

Gitelman DR, Penny WD, Ashburner J, Friston KJ, 2003 Modeling regional and psychophysiologic interactions in fMRI: the importance of hemodynamic deconvolution. Neuroimage 19 (1), 200–207. 10.1016/s1053-8119(03)00058-2. [PubMed: 12781739]

Gladwin TE, Hashemi MM, van Ast V, Roelofs K, 2016 Ready and waiting: freezing as active action preparation under threat. Neurosci. Lett 619, 182–188. 10.1016/j.neulet.2016.03.027. [PubMed: 26994781]

Glover GH, Li TQ, Ress D, 2000 Image-based method for retrospective correction of physiological motion effects in fMRI: RETROICOR. Magn. Reson. Med 44 (1), 162–167. [PubMed: 10893535]

Gozzi A, Jain A, Giovannelli A, Bertollini C, Crestan V, Schwarz AJ, et al., 2010 A neural switch for active and passive fear. Neuron 67 (4), 656–666. 10.1016/j.neuron.2010.07.008. [PubMed: 20797541]

Hagenaars MA, Oitzl M, Roelofs K, 2014 Updating freeze: aligning animal and human research. Neurosci. Biobehav. Rev 47C, 165–176. 10.1016/j.neubiorev.2014.07.021.

Henriksson L, Nurminen L, Hyvarinen A, Vanni S, 2008 Spatial frequency tuning in human retinotopic visual areas. J. Vis 8 (10), 5 1–13. 10.1167/8.10.5.

Hermans EJ, Henckens MJ, Roelofs K, Fernandez G, 2013 Fear bradycardia and activation of the human periaqueductal grey. Neuroimage 66C, 278–287. 10.1016/j.neuroimage.2012.10.063.

Herrmann MJ, Boehme S, Becker MP, Tupak SV, Guhn A, Schmidt B, et al., 2016 Phasic and sustained brain responses in the amygdala and the bed nucleus of the stria terminalis during threat anticipation. Hum. Brain Mapp 37 (3), 1091–1102. 10.1002/hbm.23088. [PubMed: 26678871]

Hutton C, Bork A, Josephs O, Deichmann R, Ashburner J, Turner R, 2002 Image distortion correction in fMRI: a quantitative evaluation. Neuroimage 16 (1), 217–240. 10.1006/nimg.2001.1054. [PubMed: 11969330]

Issa NP, Trepel C, Stryker MP, 2000 Spatial frequency maps in cat visual cortex. J. Neurosci 20 (22), 8504–8514. [PubMed: 11069958]

Joshi S, Li Y, Kalwani RM, Gold JI, 2016 Relationships between pupil diameter and neuronal activity in the locus coeruleus, colliculi, and cingulate cortex. Neuron 89 (1), 221–234. 10.1016/j.neuron.2015.11.028. [PubMed: 26711118]

Kapp BS, Frysinger RC, Gallagher M, Haselton JR, 1979 Amygdala central nucleus lesions: effect on heart rate conditioning in the rabbit. Physiol. Behav 23 (6), 1109–1117. [PubMed: 542522]

Keil A, Stolarova M, Moratti S, Ray WJ, 2007 Adaptation in human visual cortex as a mechanism for rapid discrimination of aversive stimuli. Neuroimage 36 (2), 472–479. 10.1016/j.neuroimage.2007.02.048. [PubMed: 17451974]

Keller GB, Bonhoeffer T, Hubener M, 2012 Sensorimotor mismatch signals in primary visual cortex of the behaving mouse. Neuron 74 (5), 809–815. 10.1016/j.neuron.2012.03.040. [PubMed: 22681686]

Kim JJ, Rison RA, Fanselow MS, 1993 Effects of amygdala, hippocampus, and periaqueductal gray lesions on short- and long-term contextual fear. Behav. Neurosci 107 (6), 1093–1098. 10.1037/0735-7044.107.6.1093. [PubMed: 8136063]

Koba S, Inoue R, Watanabe T, 2016 Role played by periaqueductal gray neurons in parasympathetically mediated fear bradycardia in conscious rats. Phys. Rep 4 (12) 10.14814/phy2.12831.

Kok P, Jehee JF, de Lange FP, 2012 Less is more: expectation sharpens representations in the primary visual cortex. Neuron 75 (2), 265–270. 10.1016/j.neuron.2012.04.034. [PubMed: 22841311]

Kozlowska K, Walker P, McLean L, Carrive P, 2015 Fear and the defense cascade: clinical implications and management. Harv. Rev. Psychiatr 23, 263–287. 10.1097/HRP.0000000000000065.

Lang PJ, Bradley MM, Cuthbert BN, 1997 Motivated attention: affect, activation and action In: Lang PJ, Simons RF, Balaban MT (Eds.), Attention and Orienting: Sensory and Motivational Processes. Erlbaum, Hillsdale, NJ, pp. 97–135.

LeDoux JE, Iwata J, Cicchetti P, Reis DJ, 1988 Different projections of the central amygdaloid nucleus mediate autonomic and behavioral correlates of conditioned fear. J. Neurosci 8 (7), 2517–2529. [PubMed: 2854842]

Lee, Baek J, Lu ZL, Mather M, 2014 How arousal modulates the visual contrast sensitivity function. Emotion 14 (5), 978–984. 10.1037/a0037047. [PubMed: 24932842]

Lee TS, Mumford D, 2003 Hierarchical Bayesian inference in the visual cortex. J. Opt. Soc. Am. A Opt. Image Sci. Vis 20 (7), 1434–1448. [PubMed: 12868647]

Leonova A, Pokorny J, Smith VC, 2003 Spatial frequency processing in inferred PC- and MC-pathways. Vis. Res 43 (20), 2133–2139. 10.1016/s0042-6989(03)00333-x. [PubMed: 12855249]

Liebman JM, Mayer DJ, Liebeskind JC, 1970 Mesencephalic central gray lesions and fear-motivated behavior in rats. Brain Res. 23 (3), 353–370. [PubMed: 5478303]

Lojowska M, Gladwin TE, Hermans EJ, Roelofs K, 2015 Freezing promotes perception of coarse visual features. J. Exp. Psychol. Gen 144 (6), 1080–1088. 10.1037/xge0000117. [PubMed: 26595839]

Maren S, 2001 Neurobiology of Pavlovian fear conditioning. Annu. Rev. Neurosci 24, 897–931. [PubMed: 11520922]

Nicol JR, Perrotta S, Caliciuri S, Wachowiak MP, 2013 Emotion-specific modulation of early visual perception. Cognit. Emot 27 (8), 1478–1485. 10.1080/02699931.2013.793654. [PubMed: 23705819]

Niermann HCM, Figner B, Tyborowska A, Cillessen AHN, Roelofs K, 2018 Investigation of the stability of human freezing-like responses to social threat from mid to late adolescence. Front. Behav. Neurosci 12 10.3389/fnbeh.2018.00097.

Obrist PA, 1968 Heart rate and somatic-motor coupling during classical aversive conditioning in humans. J. Exp. Psychol 77 (2), 180–193. [PubMed: 5655108]

Obrist PA, Wood DM, Perez-Reyes M, 1965 Heart rate during conditioning in humans: effects of UCS intensity, vagal blockade, and adrenergic block of vasomotor activity. J. Exp. Psychol 70 (1), 32–42. [PubMed: 14315128]

Ohman A, Wiens S, 2003 On the automaticity of autonomic responses in emotion: an evolutionary perspective In: Davidson RJ, Scherer K, Hill HH (Eds.), Handbook of Affective Sciences. Oxford University Press, New York, pp. 256–275.

Pavlov JP, 1927 Conditioned Reflexes. Oxford University Press, London.

Phelps EA, O'Connor KJ, Gatenby JC, Gore JC, Grillon C, Davis M, 2001 Activation of the left amygdala to a cognitive representation of fear. Nat. Neurosci 4 (4), 437–441. 10.1038/86110. [PubMed: 11276236]

Polack PO, Friedman J, Golshani P, 2013 Cellular mechanisms of brain state-dependent gain modulation in visual cortex. Nat. Neurosci 16 (9), 1331–1339. 10.1038/nn.3464. [PubMed: 23872595]

Purves D, Augustine GJ, Fitzpatrick D, Katz LC, LaMantia A-S, McNamara J, Williams M, 2001 Neuroscience, 2 ed Sinauer Associates, Sunderland (MA).

Roelofs K, 2017 Freeze for action: neurobiological mechanisms in animal and human freezing. Philos. Trans. R. Soc. Lond. B Biol. Sci 372 (1718) 10.1098/rstb.2016.0206.

Roelofs K, Hagenaars MA, Stins J, 2010 Facing freeze: social threat induces bodily freeze in humans. Psychol. Sci 21 (11), 1575–1581. 10.1177/0956797610384746. [PubMed: 20876881]

Rovamo J, Virsu V, Näsänen R, 1978 Cortical magnification factor predicts the photopic contrast sensitivity of peripheral vision. Nature 271 (5640), 54–56. [PubMed: 625324]

Satpute AB, Wager TD, Cohen-Adad J, Bianciardi M, Choi JK, Buhle JT, et al., 2013 Identification of discrete functional subregions of the human periaqueductal gray. Proc. Natl. Acad. Sci. U. S. A 110 (42), 17101–17106. 10.1073/pnas.1306095110. [PubMed: 24082116]

Schneiderman N, Smith MC, Smith AC, Gormezano I, 1966 Heart rate classical conditioning in rabbits. Psychonomic Sci. 6 (5), 241–242.

Sege CT, Bradley MM, Weymar M, Lang PJ, 2017 A direct comparison of appetitive and aversive anticipation: overlapping and distinct neural activation. Behav. Brain Res 326, 96–102. 10.1016/j.bbr.2017.03.005. [PubMed: 28267576]

Sereno MI, Dale AM, Reppas JB, Kwong KK, Belliveau JW, Brady TJ, et al., 1995 Borders of multiple visual areas in humans revealed by functional magnetic resonance imaging. Science 268 (5212), 889–893. [PubMed: 7754376]

Soma S, Shimegi S, Suematsu N, Sato H, 2013 Cholinergic modulation of response gain in the rat primary visual cortex. Sci. Rep 3, 1138 10.1038/srep01138. [PubMed: 23378897]

Song I, Keil A, 2013 Affective engagement and subsequent visual processing: effects of contrast and spatial frequency. Emotion 13 (4), 748–757. 10.1037/a0031553. [PubMed: 23398581]

Stolarova M, Keil A, Moratti S, 2006 Modulation of the C1 visual event-related component by conditioned stimuli: evidence for sensory plasticity in early affective perception. Cerebr. Cortex 16 (6), 876–887. 10.1093/cercor/bhj031.

Straube T, Mentzel HJ, Miltner WH, 2007 Waiting for spiders: brain activation during anticipatory anxiety in spider phobics. Neuroimage 37 (4), 1427–1436. 10.1016/j.neuroimage.2007.06.023. [PubMed: 17681799]

Thigpen NN, Bartsch F, Keil A, 2017 The malleability of emotional perception: short-term plasticity in retinotopic neurons accompanies the formation of perceptual biases to threat. J. Exp. Psychol. Gen 146 (4), 464–471. 10.1037/xge0000283. [PubMed: 28383987]

Tovote P, Esposito MS, Botta P, Chaudun F, Fadok JP, Markovic M, et al., 2016 Midbrain circuits for defensive behaviour. Nature 534 (7606), 206–212. 10.1038/nature17996. [PubMed: 27279213]

Tovote P, Fadok JP, Luthi A, 2015 Neuronal circuits for fear and anxiety. Nat. Rev. Neurosci 16 (6), 317–331. 10.1038/nrn3945. [PubMed: 25991441]

Tsuda A, Ida Y, Satoh H, Tsujimaru S, Tanaka M, 1989 Stressor predictability and rat brain noradrenaline metabolism. Pharmacol. Biochem. Behav 32 (2), 569–572. [PubMed: 2727019]

van Buuren M, Gladwin TE, Zandbelt BB, van den Heuvel M, Ramsey NF, Kahn RS, Vink M, 2009 Cardiorespiratory effects on default-mode network activity as measured with fMRI. Hum. Brain Mapp 30 (9), 3031–3042. 10.1002/hbm.20729. [PubMed: 19180557]

Vianna DM, Graeff FG, Landeira-Fernandez J, Brandao ML, 2001 Lesion of the ventral periaqueductal gray reduces conditioned fear but does not change freezing induced by stimulation of the dorsal periaqueductal gray. Learn. Mem 8 (3), 164–169. 10.1101/lm.36101. [PubMed: 11390636]

Vinck M, Batista-Brito R, Knoblich U, Cardin JA, 2015 Arousal and locomotion make distinct contributions to cortical activity patterns and visual encoding. Neuron 86 (3), 740–754. 10.1016/j.neuron.2015.03.028. [PubMed: 25892300]

Vuilleumier P, Armony JL, Driver J, Dolan RJ, 2003 Distinct spatial frequency sensitivities for processing faces and emotional expressions. Nat. Neurosci 6 (6), 624–631. [PubMed: 12740580]

Vuilleumier P, Richardson MP, Armony JL, Driver J, Dolan RJ, 2004 Distant influences of amygdala lesion on visual cortical activation during emotional face processing. Nat. Neurosci 7 (11), 1271–1278. 10.1038/nn1341. [PubMed: 15494727]

Wager TD, Nichols TE, 2003 Optimization of experimental design in fMRI: a general framework using a genetic algorithm. Neuroimage 18 (2), 293–309. 10.1016/s1053-8119(02)00046-0. [PubMed: 12595184]

Walker P, Carrive P, 2003 Role of the ventrolateral periaqueductal gray neuronsin the behavioral and cardiovascular responses to contextual conditioned fear and poststress recovery. Neuroscience 116, 897–912. 10.1016/S0306-4522(02)00744. [PubMed: 12573728]

Walker R, Deubel H, Schneider WX, Findlay JM, 1997 Effect of remote distractors on saccade programming: evidence for an extended fixation zone. J. Neurophysiol 78 (2), 1108–1119. [PubMed: 9307138]

Watson AB, Pelli DG, 1983 QUEST: a Bayesian adaptive psychometric method. Percept. Psychophys 33 (2), 113–120. 10.3758/BF03202828. [PubMed: 6844102]

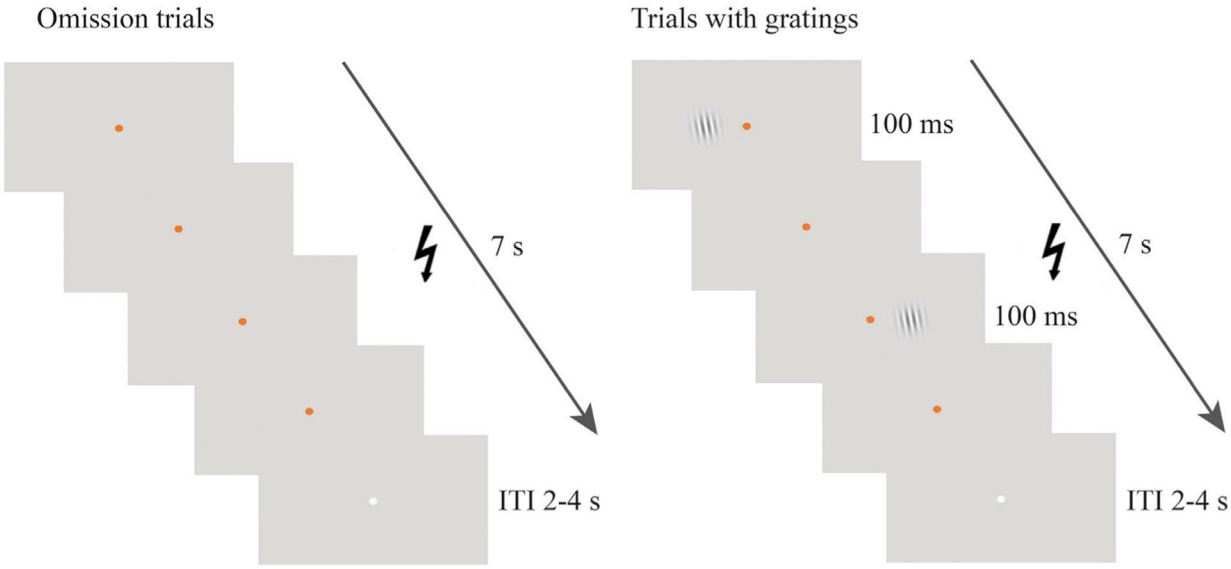

Fig. 1.

Visual task. The task consisted of omission trials and trials with gratings. Threat and safe conditions were signaled by fixation color, i.e., blue or orange, counterbalanced across participants. The figure illustrates an example of a threat condition trial, here signaled by an orange fixation, during which electric shocks could be delivered.

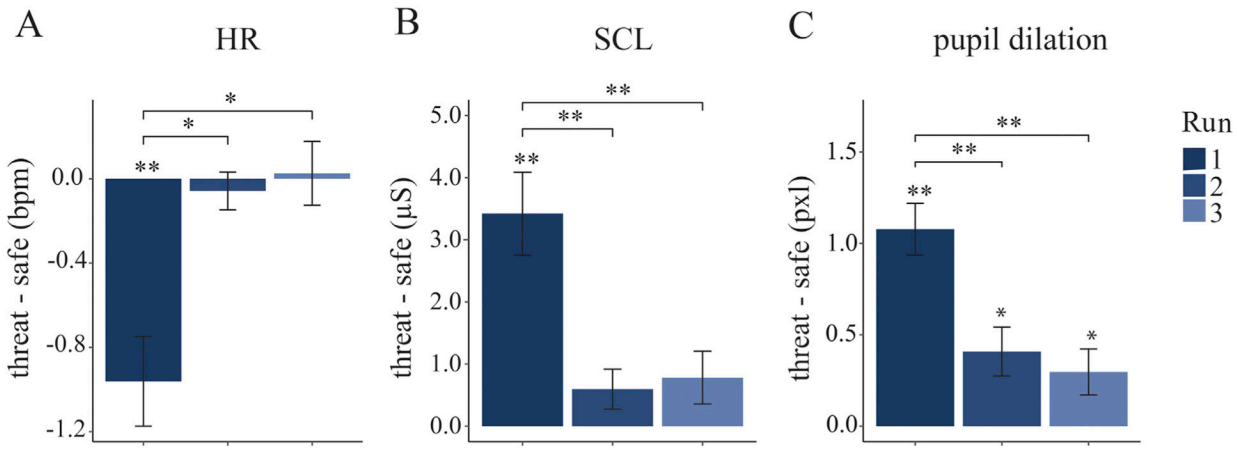

Fig. 2.

Physiological responses represented by the difference in baseline-corrected responses on threat versus safe trials for each of the three runs of the task. Differences between threat and safe conditions were strongest in run 1, with a (parasympathetically controlled) reduction in heart rate (HR) and (sympathetically controlled) increases in skin conductance levels (SCL) and pupil dilation. bpm, beats per minute; µS, microSiemens, pxl, pixels;
**, $p < .001$; *, $p < .05$.

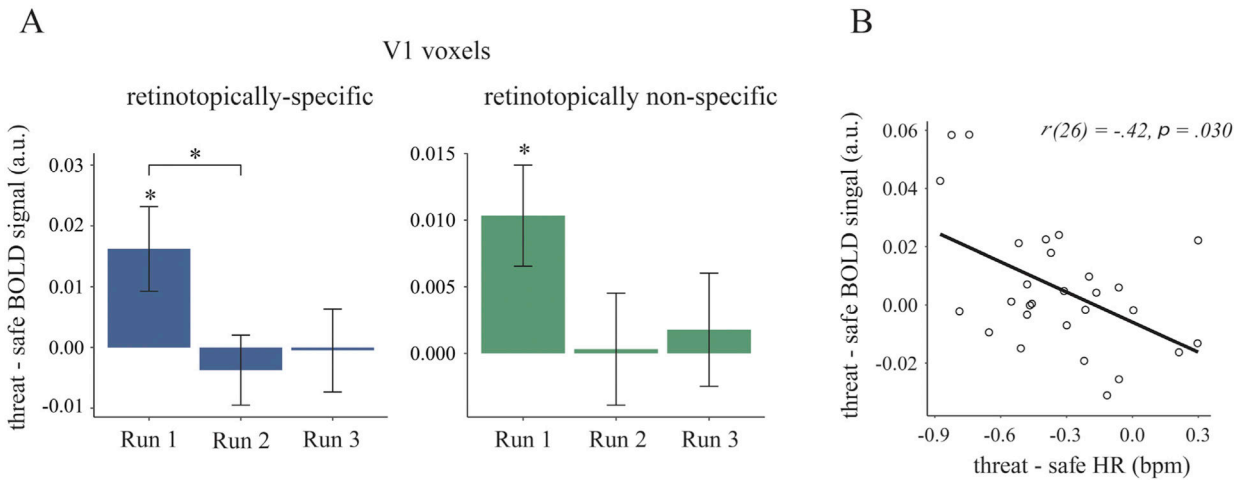

Fig. 3.

A. Neural responses in V1 in threat versus safe omission trials as a function of run number. Results show averaged BOLD responses across left and right V1, within retinotopically specific (blue) and nonspecific (green) V1 voxels. **B**. Correlation between fear bradycardia, threat-related reduction in heart rate (HR), and BOLD responses (retinotopically specific and nonspecific) in V1 in threat versus safe conditions. Error bars represent standard errors of the mean. bpm, beats per minutes;

*, $p < .05$.

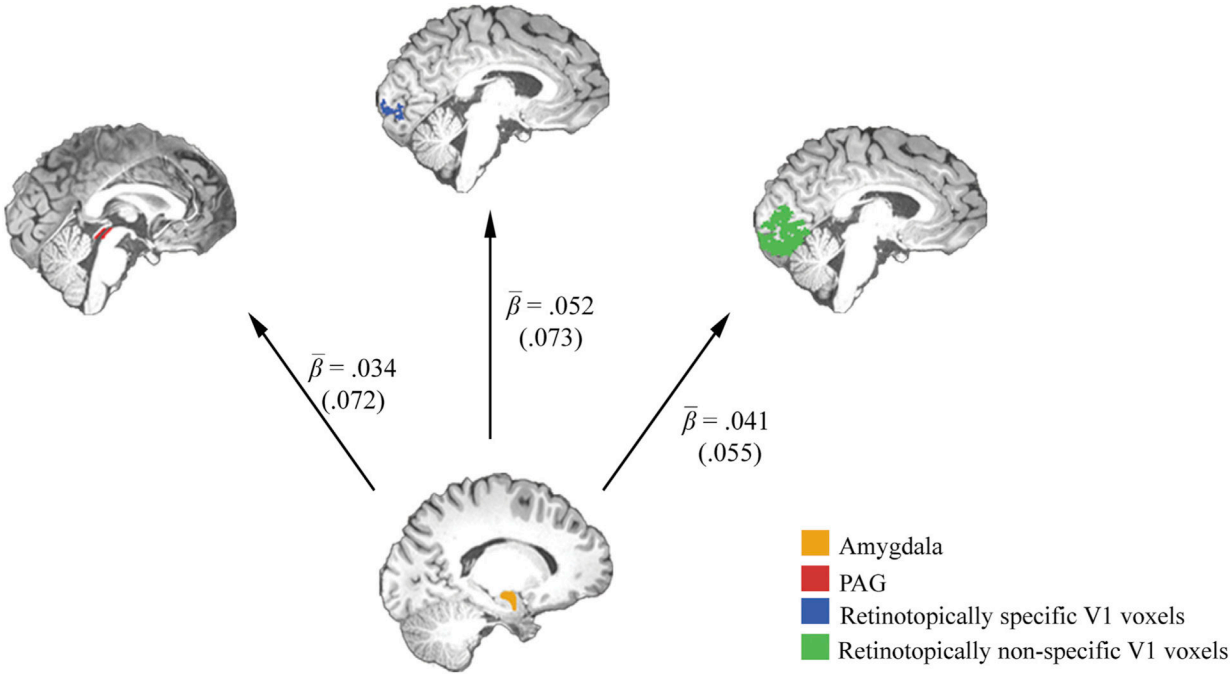

Fig. 4.

Amygdala (depicted in yellow) and its functional coupling with retinotopically specific (blue) and nonspecific (green) V1 voxels, and periaqueductal grey (PAG, in red). Beta values represent average parameter estimates for a PPI term expressing threat-related changes in connectivity with the amygdala for the three regions of interests. Values in parentheses represent standard deviations. All values were significantly different from zero (all $p < .05$).

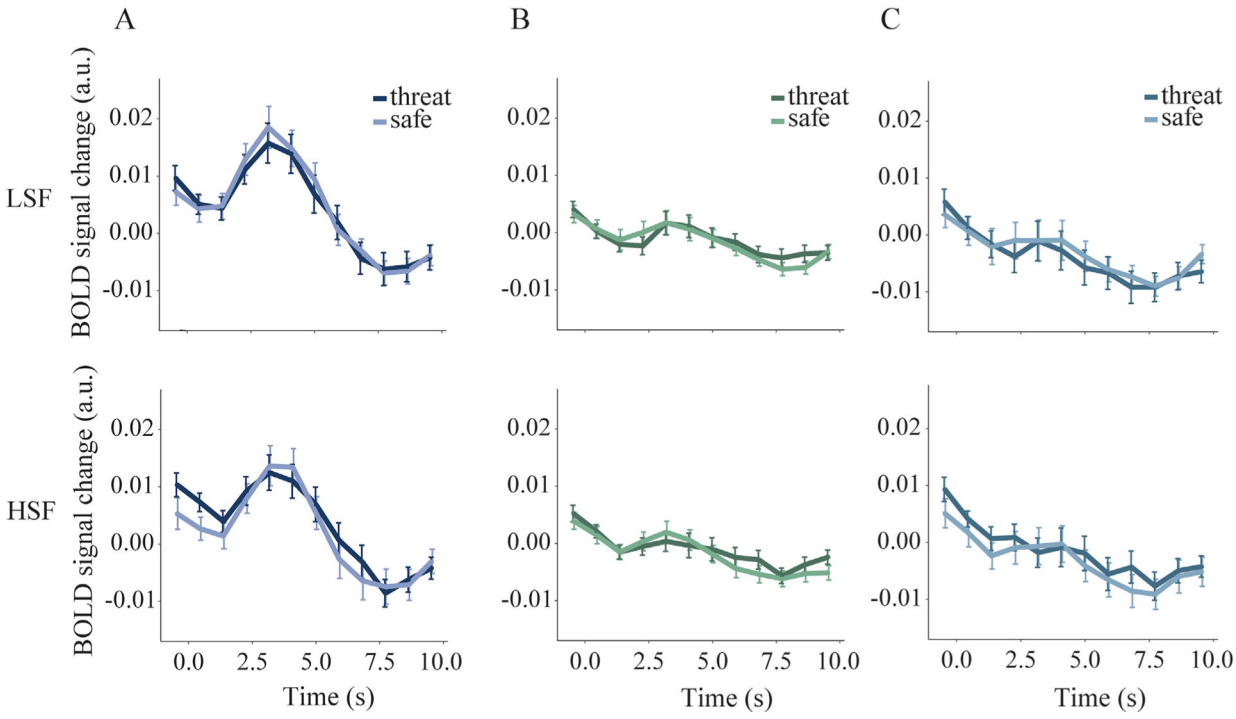

Fig. 5.

BOLD responses time-locked to the presentation of low- (LSF) and high-(HSF) spatial frequency gratings in A) retinotopically specific voxels contralateral to stimulus presentation, B) retinotopically nonspecific voxels contralateral to stimulus presentation, and C) retinotopically specific voxels ipsilateral to stimulus presentation. As expected, gratings evoked larger BOLD responses in contralateral retinotopically specific voxels compared to the two other ROIs. Within the contralateral and retinotopically specific V1 voxels, the amplitude of BOLD responses to LSF (3 cpd) and HSF (6 cpd) gratings did not differ significantly between threat and safe conditions.

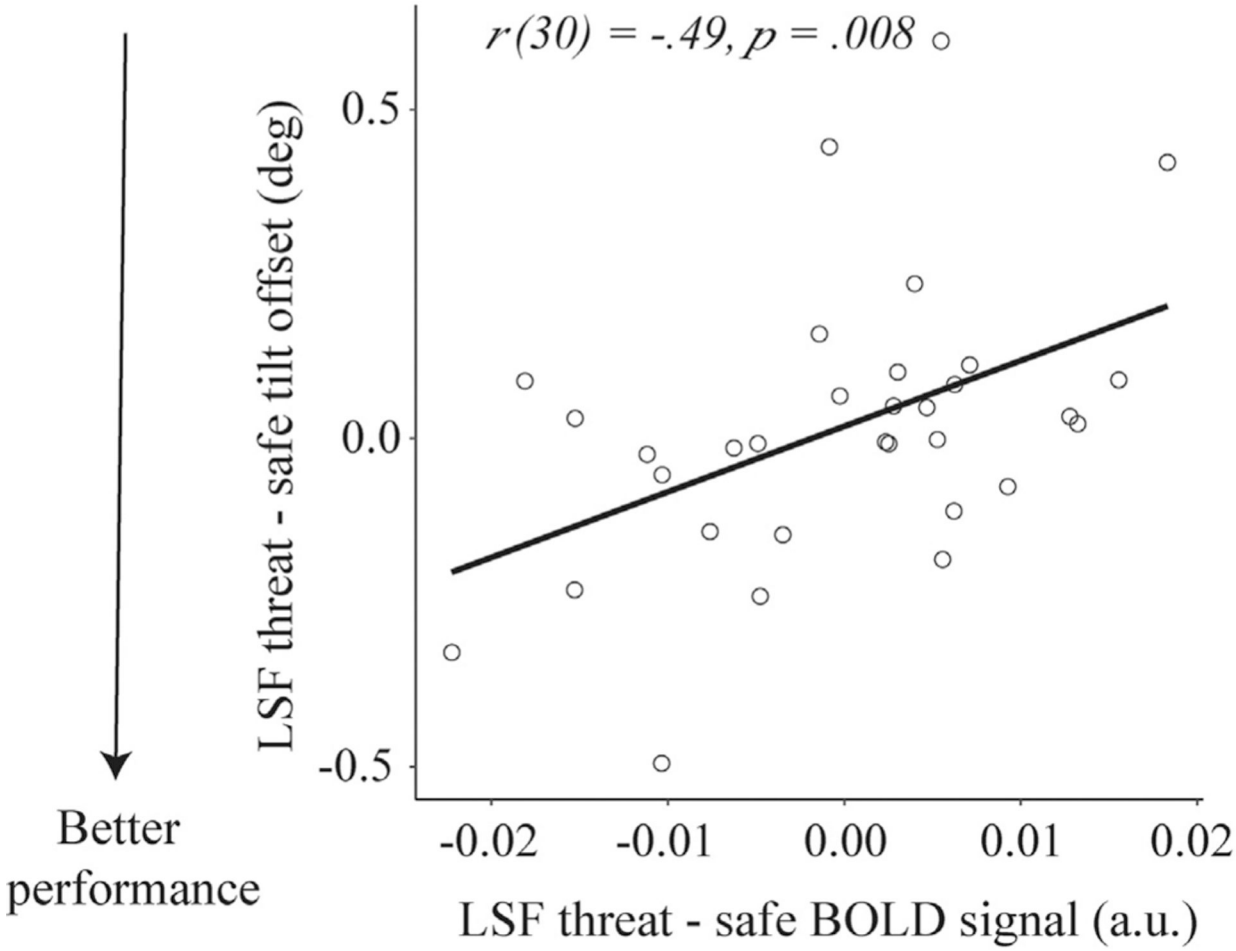

Fig. 6.

Correlation between threat-evoked responses in retinotopically specific voxels and behavioral performance to low-spatial frequency gratings (LSF) on threat versus safe trials. The facilitating effect of threat on discrimination of lowspatial frequency gratings was associated with smaller stimulus-evoked BOLD responses. deg, degrees; a.u., arbitrary units.

Table 1

Means and standard deviation (in parentheses) of tilt offset for 3 cpd (LSF) and 6 cpd (HSF) gratings under threat and safe conditions across runs.

SF	Threat condition	Run 1	Run 2	Run 3
3 cpd (LSF)	threat	2.22 (1.10)	2.09 (.96)	2.03 (.92)
	safe	2.21 (1.22)	2.11 (1.05)	2.08 (1.06)
6 cpd (HSF)	threat	3.32 (2.57)	3.11 (2.29)	3.10 (2.31)
	safe	3.43 (2.92)	3.42 (2.90)	3.31 (2.82)